Journal of Applied Polymer Science

Surface-modified MgO nanoparticle enhances the mechanical and direct-current electrical characteristics of polypropylene/polyolefin elastomer nanodielectrics

Yao Zhou, Jinliang He, Jun Hu, Bin Dang
State Key Laboratory of Power Systems, Department of Electrical Engineering, Tsinghua University, Beijing 100084, China
Correspondence to: J. L. He (E-mail: hejl@tsinghua.edu.cn)

ABSTRACT: Polypropylene (PP)/polyolefin elastomer (POE) blends and MgO/PP/POE nanocomposites were fabricated by melt blending. The morphology, mechanical, and electrical properties of the nanocomposites were investigated. Scanning electron microscopy showed that the surface-modified MgO nanoparticles were well dispersed in the polymer matrix at low loadings of less than 3 phr. X-ray diffraction demonstrated that the crystalline phases of PP in the composites were changed and that the β phase significantly increased. An examination of the electrical properties revealed that the direct-current (dc) electric breakdown strength and space-charge suppression effect were remarkably improved by the introduction of the surface-modified MgO nanoparticles. In addition, obvious enhancements in the tensile modulus and strength were obtained as a result of the synergistic toughening of the POE and MgO nanoparticles. Thus, MgO/PP/POE nanocomposites with enhanced mechanical and electrical properties have great potential to be used as recyclable insulation materials for high-voltage dc cables with large transmission capacities and high operating temperatures. © 2015 Wiley Periodicals, Inc. J. Appl. Polym. Sci. **2016**, *133*, 42863.

KEYWORDS: dielectric properties; nanoparticles; nanowires and nanocrystals; properties and characterization

Received 15 June 2015; accepted 23 August 2015
DOI: 10.1002/app.42863

INTRODUCTION

Polymer nanocomposites filled with inorganic nanoparticles, which have drawn great attention in recent years, can dramatically improve the properties of the original polymers.[1] Polymer nanocomposites seem to be able to solve current problems in many fields, such as biology, medicine, electronics, and optical and electrical materials.[2] The application of nanocomposites in electrical insulations is called *nanodielectrics*.[3] Experimental results have shown that the large interfacial zones between the nanoparticles and the polymer matrix could lead nanodielectrics to the exhibition of improved dielectric breakdown strength, space-charge suppression, direct-current (dc) volume resistivity, mechanical strength, dielectric permittivity, and partial discharge resistance.[4] Because polymer nanodielectrics possess not only the aforementioned advantages but also ease of processing, they are excellent candidates for insulation applications, in particular, high-voltage power cable insulations.

A promising application of polymer nanodielectrics is as insulation for electric power transmission cables. The huge demand on electric power cables with higher transmission capacities inevitably leads to higher operating temperatures, and this requires that insulation materials should not only have excellent electrical properties but also exhibit good thermal and mechanical properties.[5] Then, the determination of a method improve and balance these desired properties becomes a difficult problem. Undoubtedly, polymer nanocomposites should be a good choice.[6] Many works have been done to develop novel nanodielectrics with excellent integrated performance for high-voltage direct-current (HVDC) power transmission cables.[7–10] Also, many preparation strategies for the fabrication of high-performance dielectric nanocomposites have been developed; these include solution blending,[11] *in situ* polymerization,[12] and oligomer grafting.[13] Among these strategies, *in situ* polymerization is the best way to uniformly disperse the nanoparticles and give them good mechanical and electrical performances. However, for the insulation applications of extruded power cables, melt blending is more applicable in industrial production.

Low-density polyethylene (LDPE) is the most popular polymer matrix in nanodielectrics because of its simple molecular structure, but LDPE is not suitable for practical applications because of its low thermal stability, low operating temperature, and poor mechanical properties. Therefore, LDPE is crosslinked into crosslinked polyethylene (XLPE) with various methods, including peroxide crosslinking, silane crosslinking, and irradiation crosslinking, to improve the thermal stability and mechanical

strength of LDPE through the formation of crosslinked macromolecular networks in XLPE.[14] However, the crosslinking process also results in thermoset material; this makes it very difficult to recycle XLPE. As environmental protection and sustainable development are becoming more important than ever, the development of novel ecofriendly insulation materials for next-generation recyclable HVDC cables is of great importance.

Because of its high operating temperature, excellent dc dielectric properties, and thermoplastic nature, polypropylene (PP) has been considered to be a good candidate for recyclable cable insulation materials, but the mechanical properties of PP should be improved because PP is very easy to fracture. To improve the mechanical properties of PP, copolymerization with other olefins,[15] blending with thermoplastic polyolefins or polyolefin elastomers (POEs),[16] and the addition of inorganic nanofillers[17] are usually used. In our previous study,[18] POE was used to improve the mechanical properties of PP by melt blending, and positive results were received, but space-charge accumulation under a dc electric field was still a problem, and this was very unfavorable. The accumulation of space charge caused a distortion of the local electric field and severely reduced the breakdown strength and insulation life.[19] Fortunately, recent advances in nanodielectrics have shown that the introduction of a small amount of inorganic nanoparticles into polymers can effectively suppress space-charge accumulation[20] and improve the electrical properties.[21] However, the dispersion of nanoparticles in the polymer matrix is still a challenge, and bad dispersion means negative results. Many methods have been adopted to obtain good dispersion; these include sonication,[22] shear mixing,[23] and chemical surface functionalization with a surface-active agent or silane coupling agent.[20] Among them, chemical surface functionalization with a silane coupling agent is widely used.[24] The surface modification process changes the surface physicochemical characteristics of the nanoparticles to improve the compatibility between the nanoparticles and the polymer matrix.[25]

In this study, MgO/PP/POE nanocomposites with different MgO nanofiller contents were prepared by melt blending. To realize uniform dispersion and good compatibility, the MgO nanoparticles were surface-modified with a silane coupling agent. The dispersion of the MgO nanoparticles in the polymer matrix and the crystalline phases and the mechanical and electrical properties of the nanocomposites were investigated. The influence of the surface-modified MgO nanoparticles on the properties of the PP/POE matrix was investigated in detail, and the optimal content of MgO nanoparticles was determined experimentally. The relationship between the structure and the mechanical and electrical properties, in particular, the space-charge accumulation of the nanocomposites, is discussed. The aim of this study was to develop a novel recyclable insulation material for power cables.

EXPERIMENTAL

Materials

Spherical MgO nanoparticles with an average diameter of 50 nm, a special surface area of 70 ± 15 m^2/g, and a purity of 99.9% were obtained from Aladdin Industrial, Inc. (China). 3-aminopropyltriethoxysilane (KH550) and ethanol were all analytical grade and were purchased from Sinopharm Chemical Reagent Co., Ltd. (China). PP (F401) was purchased from Panjin Ethylene Co., Ltd. (China) and was additive free and had an isotacticity of 97%, a density of 0.910 g/cm^3, and a melt flow index of 1.7–3.1 g/10 min. POE (8150) was purchased from DuPont Dow and was a kind of ethylene–octene copolymer with a density of 0.868 g/cm^3 and a melt flow index of 0.5 g/10 min. All of the chemicals were used as received without any further purification.

Surface Modification of the MgO Nanoparticles

The surface modification of the MgO nanoparticles was carried out with the following method. The MgO nanoparticles were vacuum-dried at 373 K for 12 h before surface modification. Then, 10 g of MgO nanoparticles was dispersed in ethanol by sonication for 30 min. A 3-aminopropyltriethoxysilane/ethanol mixture was slowly added to the nanoparticle/ethanol mixture by a dropping funnel. Then, the mixture was put into an oil bath at about 343 K and magnetically stirred for 12 h. The resulting slurry was centrifuged at 6000 rpm for 6 min and then washed with fresh ethanol three times to remove excess coupling agent. Finally, the surface-modified nanoparticles were dried in a vacuum oven at 333 K for 12 h. To make a comparison between the unmodified and modified MgO nanoparticles, the unmodified nanoparticles were prepared in the same way except without the addition of the coupling agent.

Preparation of the PP/POE/MgO Nanocomposites

The surface-modified MgO nanoparticles and PP and POE pellets were mixed at the same time with an RM-200C torque rheometer (HAPRO, Harbin, China) at 453 K with a rotor speed of 60 rpm for 15 min. The content of POE in the PP/POE polymer matrix was 30 wt %, and the weight fractions of the surface-modified MgO nanoparticles in the nanocomposites were 0, 0.5, 1, 3, and 5 phr, respectively (where 1 phr indicates 1 g of surface-modified MgO nanoparticles in 100 g of a PP/POE blend). Film samples with different thicknesses used for property measurements were obtained with compression molding at 473 K for 7 min under a pressure of around 20 MPa. Then, the film samples were cooled to room temperature under the same pressure. To eliminate the influence of different thermal histories and residual internal stresses, all of the film samples were annealed in a vacuum oven at 408 K for 2 h and cooled to room temperature. All of the samples were stored in a vacuum drier to exclude the influence of moisture.

Characterization

Thermogravimetric analysis (TGA) was performed on both the surface-modified MgO nanoparticles and the nanoparticles without treatment with a TA Q500 instrument. The typical sample size for TGA was 5 mg, and samples were analyzed from 303 to 973 K at a heating rate of 10 K/min under flowing dry air.

The chemical structures of the surface-modified MgO nanoparticles were analyzed by Fourier transform infrared spectroscopy (Nicolet 6700) between 400 and 4000 cm^{-1}. The samples were analyzed at a 2-cm^{-1} resolution, and the results were averaged over 10 scans. Before measurement, the background atmosphere was measured and subtracted from each spectrum.

The nanoparticle dispersion and morphologies of the composites were observed via field emission scanning electron microscopy (FESEM; Zeiss Sigma, Germany). Samples for FESEM observation were first fractured in liquid nitrogen and then sputtered with gold on the cross sections to prevent charge accumulation during observation.

Wide-angle X-ray diffraction measurements were performed on an automatic diffractometer (Rigaku D/MAX-2550HB+/PC, Rigaku Corp., Japan) at room temperature with nickel-filtered Cu target Kα radiation at 40 kV and 20 mA. The tests were performed in the range 10–50° at a scanning rate of 3°/min.

Tensile tests of the composites were carried out on a tensile tester (Z010, Zwick/Roell, Germany) according to ASTM D 638 with a fixed speed of 50 mm/min at room temperature. Dumbbell-shaped specimens with a cross section of 4 × 0.5 mm^2 and a gauge length of 20 mm were prepared for measurements. Five specimens for each sample were used for repeat measurements, and the arithmetic mean of the values obtained for each sample is reported as the average value for the particular properties of each sample.

The dc breakdown tests were done with a dielectric strength tester with a 10-mm ball-to-ball electrode (HT-50, Guilin Electrical Equipment Scientific Research Institute, China) at room temperature. The composite films of about 120 μm were placed between two sphere electrodes and immersed in silicone oil to prevent surface flashover. A dc ramp voltage with a ramping rate of 1 kV/s was applied across the electrodes until the films were broken down. Sixteen specimens were tested for each sample. The breakdown test data were treated with the two-parameter Weibull statistical distribution method. The two-parameter Weibull statistical distribution can be written as follows:

$$P=1-\exp\left[-\left(\frac{E}{E_0}\right)^{\beta}\right] \quad (1)$$

where E is the experimental electric breakdown strength, β is the shape parameter reflecting the data scatter, and E_0 is the characteristic breakdown strength and represents the breakdown strength at 63.2% cumulative breakdown probability. E_0 is usually used to compare the electric breakdown strength of different samples, and P is the cumulative probability of breakdown. According to IEEE 930-2004, a simple but good approximation for the probability of breakdown can be written as follows:

$$P_i=\frac{i-0.44}{n+0.25}\times 100\% \quad (2)$$

where P_i is the cumulative probability of ith breakdown data, i is the ith result when the breakdown data of E are sorted in ascending order and n is the number of specimens of each sample ($n=16$ in this study). dc volume resistivity measurements were performed with an electrometer with a standard three-electrode system (Keithley 6517A). The thin-film samples (thickness ≈ 120 μm) for dc volume resistivity measurements were first electrically short-circuited for 5 min to eliminate internal charges, and then, a constant dc electric field of 5 kV/mm was applied on the samples for 5 min, and the charging current was recorded. For each sample, five specimens were used for repeat measurements, and error bars were calculated according to the results.

A Novolcontrol Alpha-A high-performance frequency analyzer (GmbH, Germany) was used to measure the permittivity and the loss of the nanocomposites. All of the measurements were carried out in the frequency range 1–10^6 Hz at room temperature under a 1.0-V alternating-current voltage. The samples were evaporated with a gold layer on both surfaces to serve as electrodes.

The pulse electroacoustic method was used to measure the space-charge distribution within the film samples (thickness ≈ 210 μm). An electric pulse with an amplitude of 800 V and a duration of 5 ns was applied to the samples. Silicone oil was used to ensure good acoustic contact between the samples and the electrodes. All of the measurements were performed under −40 kV/mm dc electric field for 30 min at room temperature, and the space-charge distributions during polarization process were recorded. We confirmed the reproducibility of the experiment profile by repeating the experiments at least three times for each sample.

RESULTS AND DISCUSSION

Characterization of the Surface-Modified MgO Nanoparticles

Figure 1 shows the Fourier transform infrared spectrum of the MgO nanoparticles with and without surface modification, which are represented by MgO–KH550 and MgO, respectively. Compared with the spectrum of the unmodified MgO nanoparticles, new absorption peaks appeared at 2920 and 2850 cm^{-1} (stretching vibrations of —CH_2 groups), and new absorption bands appeared at 1000–1200 cm^{-1} (stretching vibrations of —Si—O groups and —C—N groups) in the surface-modified MgO nanoparticles;[26] this indicated that 3-aminopropyltriethoxysilane was successfully grafted onto the surface of the MgO nanoparticles. There was also a decrease in the absorption peak at 3456 cm^{-1} in the surface-modified MgO nanoparticles; this was attributed to the reduction of —OH absorbed on the surface of MgO due to the reaction with —OC_2H_5 in the silane coupling agent. The

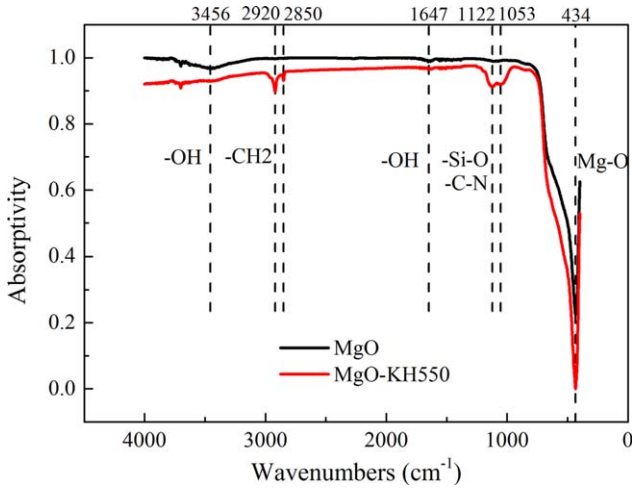

Figure 1. Fourier transform infrared spectra of MgO nanoparticles with and without surface modification. [Color figure can be viewed in the online issue, which is available at wileyonlinelibrary.com.]

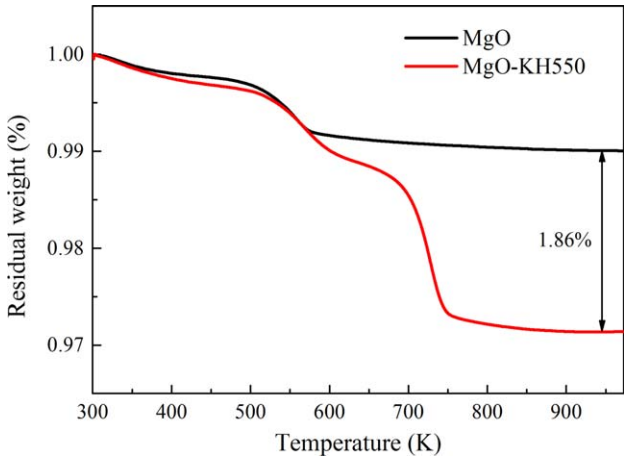

Figure 2. TGA curves of MgO nanoparticles with and without surface modification. [Color figure can be viewed in the online issue, which is available at wileyonlinelibrary.com.]

results of TGA provided further evidence for the successful surface modification of the MgO nanoparticles. As shown in the TGA curves in Figure 2, the weight loss of the surface-modified MgO nanoparticles was much bigger than that of the unmodified nanoparticles (ca. 1.86% higher). The weight loss around 550 K of the unmodified nanoparticles was possibly associated with leaving lattice hydroxyls.[27] In contrast, the TGA behavior of the surface-modified nanoparticles was more complex; this was attributed to the loss of organics grafted onto the surface of the nanoparticles during surface modification. This further proved that the silane coupling agent was successfully grafted onto the MgO nanoparticles.

Microstructural Characterization of the MgO/PP/POE Nanocomposites

Good compatibility between nanoparticles and the polymer matrix can result in excellent mechanical and electrical properties, so the MgO nanoparticles were surface-modified with a silane coupling agent.[28,29] FESEM was used to examine the dispersion of MgO nanoparticles in the PP/POE matrix, and Figure 3 shows the FESEM images of the MgO/PP/POE nanocomposites with 0-, 0.5-, 1-, 3-, and 5-phr MgO nanoparticles, respectively. The small black box at the bottom left corner of each image presents the local amplified area, which shows the typical dimensions of the nanoparticles in each sample. There are round holes with diameters of several micrometers in all of the figures; these were attributed to the removal of POE while the samples were fractured in liquid nitrogen. In our previous study, we examined the compatibility of PP and POE and found that PP and POE had a certain degree of compatibility but were not perfectly compatible.[18] Among the morphologies of different nanocomposites, the composites with less than 3-phr MgO nanoparticles displayed a good visual distribution. This revealed that the MgO nanoparticles were well dispersed in the PP/POE matrix. Although small aggregates of individual nanoparticles were observed in all of the samples, it was clear that the MgO nanoparticles dispersed well with little aggregation at filler content of less than 3 phr, and the dimensions of small aggregates were estimated to be less than 200 nm and appeared to be clumps of three to five individual nanoparticles. The good dispersion of the MgO nanoparticles were attributed to the surface modification with the silane coupling agent; this resulted in a reduced surface free energy, changes in the physicochemical characteristics and better adhesion properties of the nanoparticles. Comparatively, the dispersion and compatibility of the nanocomposite with a larger filler content of 5 phr were poor, and there were large amounts of aggregates with dimensions of around 1 μm or even larger; this was due to the large amount of nanoparticles introduced. Figure 3(e) shows that there were numerous voids inside the large aggregates; these voids made it easy for the formation of defect sites and deteriorated the mechanical and electrical properties of the nanocomposites. The results of scanning electron microscopy observation just suggest that only a suitable content of the MgO nanoparticles introduced into the PP/POE matrix could obtain uniform dispersion and good compatibility.

PP is a polymorphic material, which has a complex microstructure and can crystallize in monoclinic (α), trigonal (β), orthorhombic (γ), and smectic modifications.[30] Among the different crystalline phases, the α-phase is the most possible phase; it is thermodynamically stable and predominant under common processing conditions. The β phase occurs more rarely because of a lower stability than α phase, but a high content of β phase can be achieved under special conditions, such as crystallization under a temperature gradient and in the presence of β nucleators.[31–33] Of these different crystalline phases, the β phase is technically important because of its increased impact strength and thermoformability.[34] Therefore, it is important to investigate how MgO nanoparticles affect the crystalline phases of PP, and thus, X-ray diffraction is used to characterize the crystalline phases of PP in the MgO/PP/POE nanocomposites. As is shown in Figure 4, each type of nanocomposite showed a typical diffractogram of the α phase; these were at 2θs of 14.04, 16.88, 18.53, 21.11, and 21.85°, which corresponded to the (110), (040), (130), (111), and (130) planes, respectively.[35] However, with the introduction of MgO nanofillers, a new diffraction peak appeared at $2\theta = 16.02°$, which increased with the MgO nanofiller content and was associated with the (300) plane of the β phase. The appearance and increase of the β phase PP indicated that the MgO nanoparticles could act as β nucleators, and the crystalline phases of PP changed. The increase of the β phase in PP was very conducive to improvements in the mechanical properties of the nanocomposites; this was further verified with tensile tests. In addition, the diffraction peak at $2\theta = 42.90°$ referred to the (200) plane of the MgO crystal;[36] it increased with the MgO nanofiller content. This further proved that the MgO nanoparticles were introduced into the composites at the expected filler content.

Mechanical Behavior of the MgO/PP/POE Nanocomposites

The stress–strain curves of the PP/POE blends and MgO/PP/POE nanocomposites with 0.5-, 1-, 3-, and 5-phr surface-modified nanoparticles are shown in Figure 5(a). The corresponding obtained values of the tensile strength and elongation at break are shown in Figure 5(b). With the increased MgO nanofiller content, the tensile strength and elongation at break of the nanocomposites with 1-phr surface-modified MgO nanoparticles reached the maximum value and then decreased.

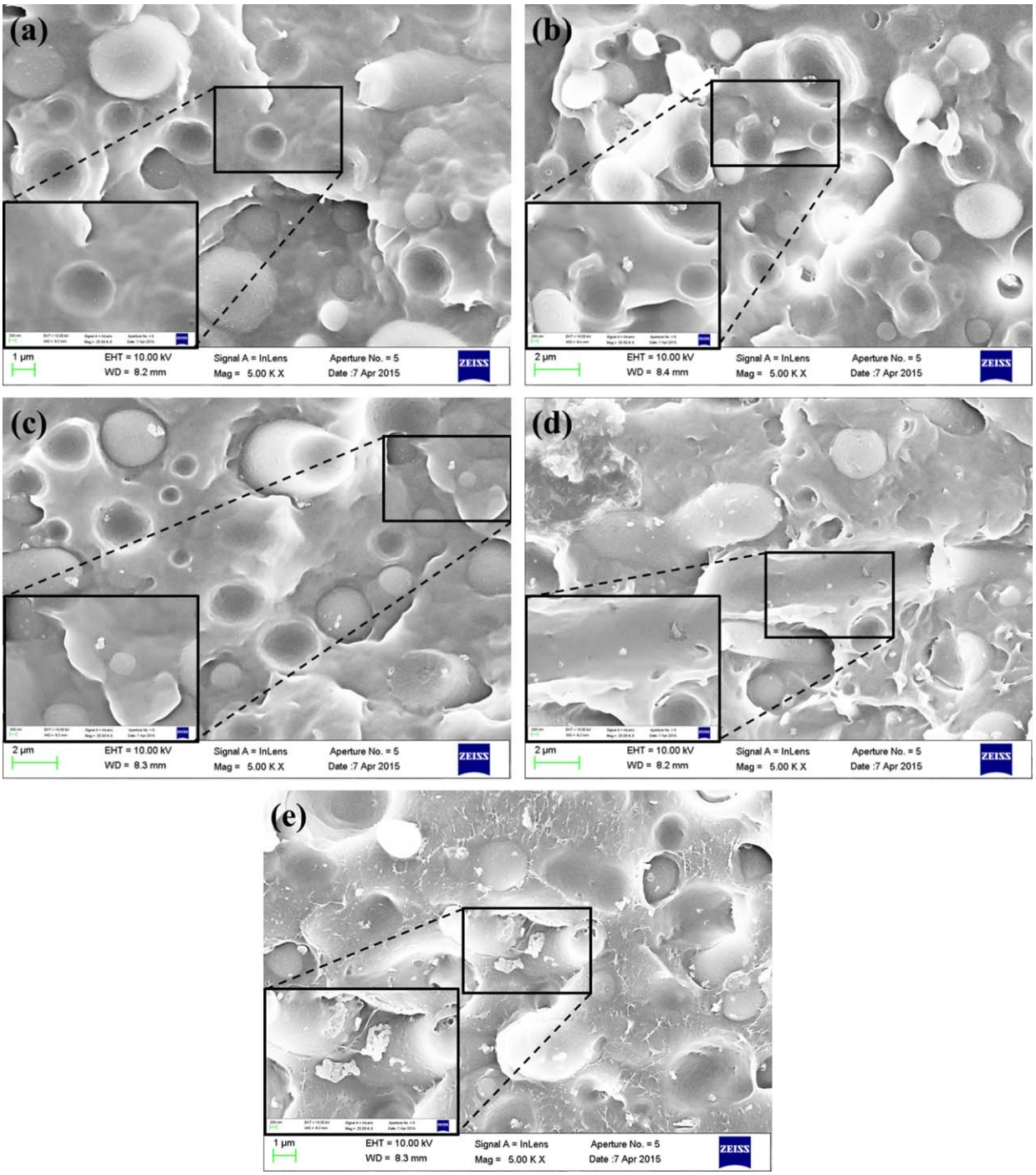

Figure 3. FESEM images of the MgO/PP/POE nanocomposites filled with surface-modified MgO nanoparticles: (a) 0, (b) 0.5, (c) 1, (d) 3, and (e) 5 phr. [Color figure can be viewed in the online issue, which is available at wileyonlinelibrary.com.]

Compared with the tensile strength of 15.4 MPa for the PP/POE blends with 30 wt % POE, the addition of 1-phr MgO nanoparticles led to an obviously enhanced tensile strength of 21.1 MPa. Also, a synergistic toughening effect of the POE and MgO nanoparticles was observed in the elongation at break of the MgO/PP/POE nanocomposites. The elongation at break of the nanocomposites increased from 865% for the PP/POE blends with 30 wt % POE to 1110% for the MgO/PP/POE nanocomposites with 1-phr MgO nanoparticles. The enhancement of the mechanical properties was attributed to the huge nanoparticle–polymer interfaces in the nanocomposites, which had different properties than the original polymer matrix, and similar results have been reported in previous studies.[37–40] Furthermore, the organic segment of the coupling agent KH550 was entwined with the segments of PP, and this ensured good compatibility and interfacial adhesion between the nanoparticles and the polymer matrix, so the mechanical properties were improved. In addition, as shown previously, the introduction of

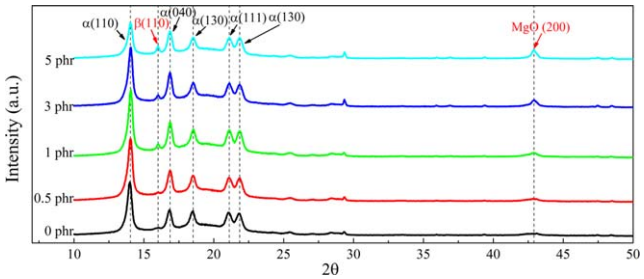

Figure 4. X-ray diffraction curves of the MgO/PP/POE nanocomposites with different MgO nanofiller contents. [Color figure can be viewed in the online issue, which is available at wileyonlinelibrary.com.]

MgO nanoparticles changed the crystalline phases, and the β-phase PP was significantly increased; this was very conducive to improvements in the mechanical properties, as the flexibility of β-PP is superior to that of α-PP.[34] However, when a content of more than 3 phr of MgO nanoparticles was introduced, the tensile strength and elongation at break decreased continuously. The degeneration of the mechanical properties was attributed to the gradual aggregation of MgO nanoparticles, and this easily resulted in defects and stress concentration.

Dielectric Properties of the MgO/PP/POE Nanocomposites

Figure 6(a) shows the Weibull plots of the dc electric breakdown strength of the MgO/PP/POE nanocomposites with different MgO nanofiller contents. The dc breakdown strength increased at low loadings of MgO nanoparticles, reached its maximum value at 3 phr, and then decreased. Figure 6(b) summarizes the characteristic breakdown strengths of the nanocomposites. The maximum characteristic breakdown strength was 370 kV/mm for the nanocomposite with 3-phr MgO nanoparticles; this was about 15% higher than that of the PP/POE blends (323 kV/mm) and was also much higher than that of the typical XLPE of 300 kV/mm.[41] The increased dc breakdown strength was attributed to the surface modification of the MgO nanoparticles; this ensured good interfacial adhesion properties and compatibility between the nanoparticles and the polymer matrix and resulted in a uniform dispersion of the nanoparticles. Previous studies have shown that the insulation failure under a dc electric field is closely related to space-charge accumulation, and the introduction of surface-modified nanoparticles could suppress space-charge accumulation.[42,43] As shown later in Figure 9, the introduction of MgO nanoparticles

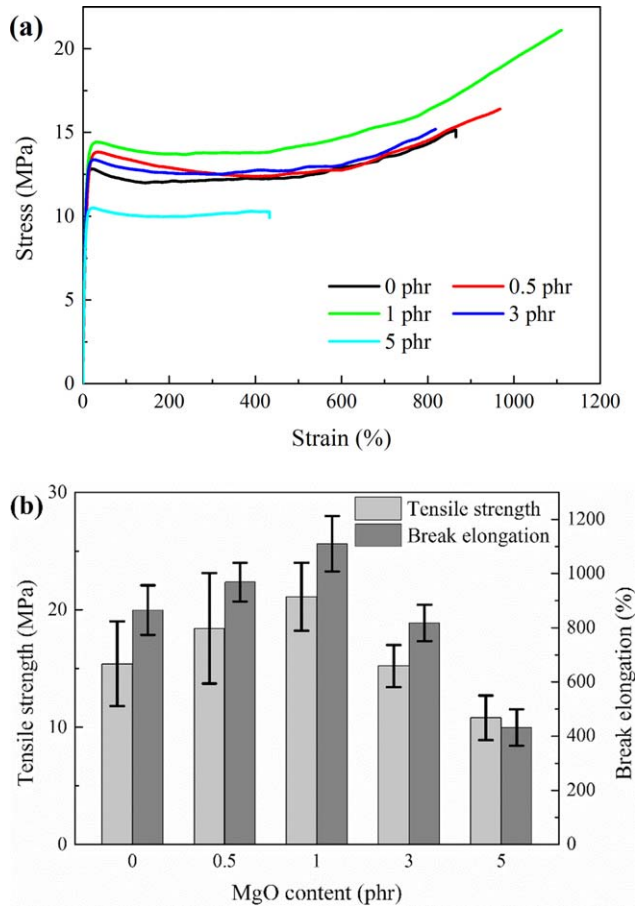

Figure 5. Mechanical properties of the MgO/PP/POE nanocomposites: (a) typical stress–strain curves and (b) tensile strength and elongation at break versus the MgO nanofiller content. [Color figure can be viewed in the online issue, which is available at wileyonlinelibrary.com.]

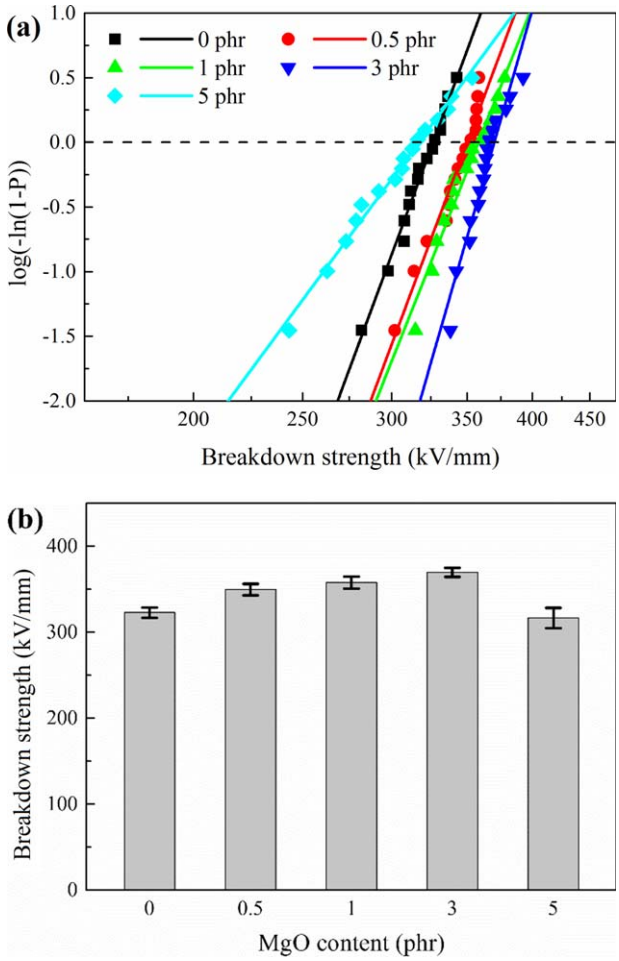

Figure 6. (a) Weibull plots of the breakdown strength and (b) characteristic breakdown strength of the MgO/PP/POE nanocomposites with different MgO nanofiller contents. [Color figure can be viewed in the online issue, which is available at wileyonlinelibrary.com.]

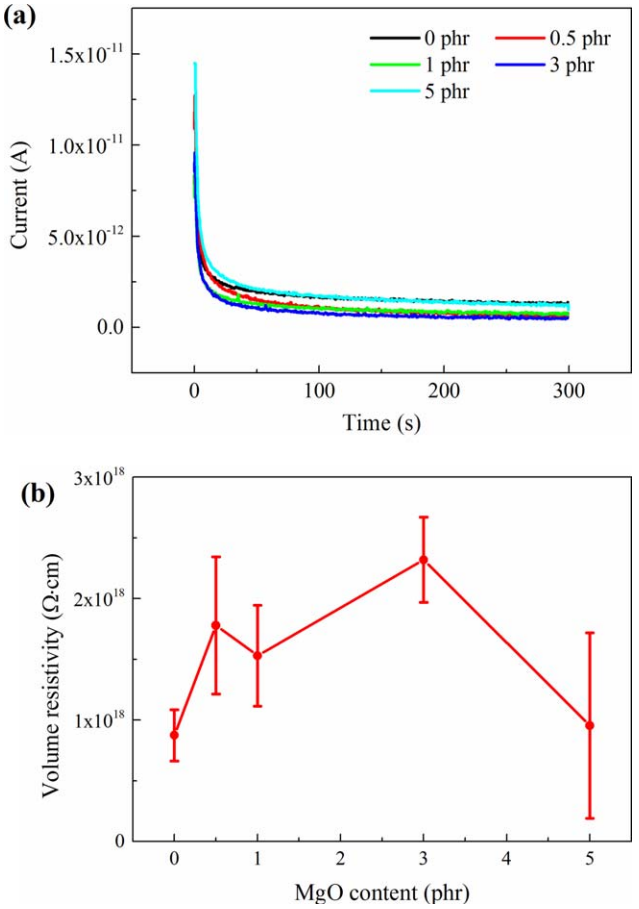

Figure 7. (a) Time dependence of the dc charging current of the MgO/PP/POE nanocomposites with different MgO nanofiller contents and (b) dc volume resistivity versus the MgO nanofiller content. [Color figure can be viewed in the online issue, which is available at wileyonlinelibrary.com.]

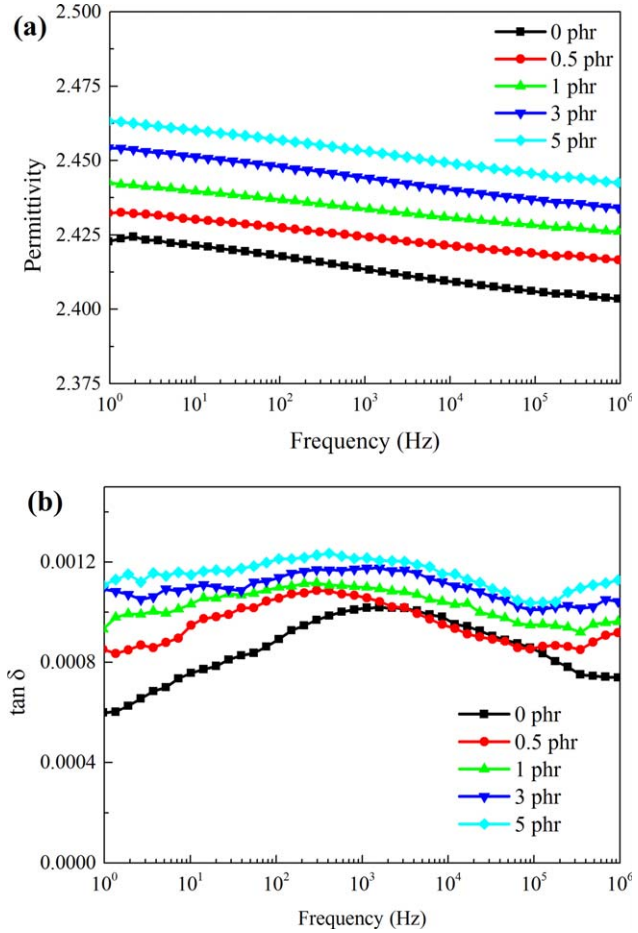

Figure 8. (a) Frequency dependence of the dielectric permittivity and (b) dielectric loss tangent of the MgO/PP/POE nanocomposites with different MgO nanofiller contents. [Color figure can be viewed in the online issue, which is available at wileyonlinelibrary.com.]

effectively suppressed the space-charge accumulation in the MgO/PP/POE nanocomposites, so the dc breakdown strength increased. However, the breakdown strength did not continue to increase when the nanoparticle content was beyond 5 phr and even lower than that of the PP/POE blends. The reduction of the dc breakdown strength was due to aggregation of nanoparticles. As shown in Figure 3(e), there were large aggregates with dimensions of around 1 μm or even larger in the nanocomposites with 5-phr MgO, and these micrometer particles acted as defects and became the weakest point in the bulk of samples; this caused the initial breakdown.[26] The results of dc breakdown tests revealed that the 3-phr surface-modified MgO nanoparticles introduced into the PP/POE blends had the most desirable dc dielectric properties.

For insulation applications, dielectric strength is not the only determinate factor; the dc volume resistivity, which determines dielectric loss under a dc electric field, is also very important. Figure 7(a) describes time dependence of the dc leakage currents of the MgO/PP/POE nanocomposites, and the corresponding dc volume resistivities, calculated according to the leakage currents at 5 min, are shown in Figure 7(b). The leakage currents of the PP/POE blends and MgO/PP/POE nanocomposites all decayed very quickly and reached their steady state within 5 min. When the concentration of MgO nanoparticles was lower than 3 phr, the dc volume resistivity increased with the nanoparticle content, and the dc volume resistivity of the nanocomposite with 3-phr MgO nanoparticles was over two times that of the PP/POE blends. However, when the nanofiller content reached 5 phr, the dc volume resistivity decreased sharply and was even lower than that of the PP/POE blends; similar results were reported for MgO/LDPE nanocomposites.[44] Under a dc electric field, the MgO nanoparticles could polarize and generate electric potential wells at the interface.[45] These electric potential wells could trap charge carriers and reduce the charge carrier mobility; this resulted in an improved dc volume resistivity. At low loadings of MgO nanoparticles, the number of potential wells was closely related to the nanofiller content, and a higher content meant more potential wells and a higher dc volume resistivity. When a large amount of MgO nanoparticles were introduced (e.g., 5 phr in this study), serious aggregates of MgO nanoparticles [shown in Figure 3(e)] and bad adhesion properties resulted in reduced potential wells and a lower dc volume resistivity.[46] Because of the much lower volume resistivity compared with the polymer matrix, large aggregates of MgO

nanoparticles also acted as conduction impurities and increased the dc volume resistivity of the nanocomposites. As shown in Figure 7(b), the error bar of the dc volume resistivity at 5 phr was comparatively larger; this further illustrated that the nanocomposite with 5-phr MgO nanoparticles was not uniform.

Figure 8 gives the frequency-dependent dielectric permittivity and dielectric loss tangent of the PP/POE blends and MgO/PP/POE nanocomposites. Compared with PP/POE blends, all of the nanocomposites showed a slightly enhanced dielectric permittivity; this was attributed to the higher dielectric permittivity of the MgO nanoparticles. For both the PP/POE blends and MgO/PP/POE nanocomposites, the dielectric permittivity was very stable with the variation of frequency; this indicated that the material had a wide applicable frequency range. As for the dielectric loss tangent, the differences between different materials were marginal and dependent on the content of MgO nanoparticles. The introduction of MgO nanoparticles increased the dielectric loss tangent, and a higher content of MgO resulted in a higher dielectric loss. However, the value of the dielectric loss tangent was very small and on the order of 10^{-3}; this indicated excellent dielectric properties.

Space-Charge Characterization of the MgO/PP/POE Nanocomposites

Space charge is one of the most important factors affecting the insulation behaviors of dielectric materials under dc electric stress. Previous studies of space-charge behavior under a dc electric field have shown that the accumulation of space charge causes a distortion of the local electric field and, thus, partial discharge and then insulation failure.[19] So space-charge suppression is of great importance for insulation materials, and methods for space-charge suppression should be investigated. Recent studies in nanodielectrics have proven that the introduction of

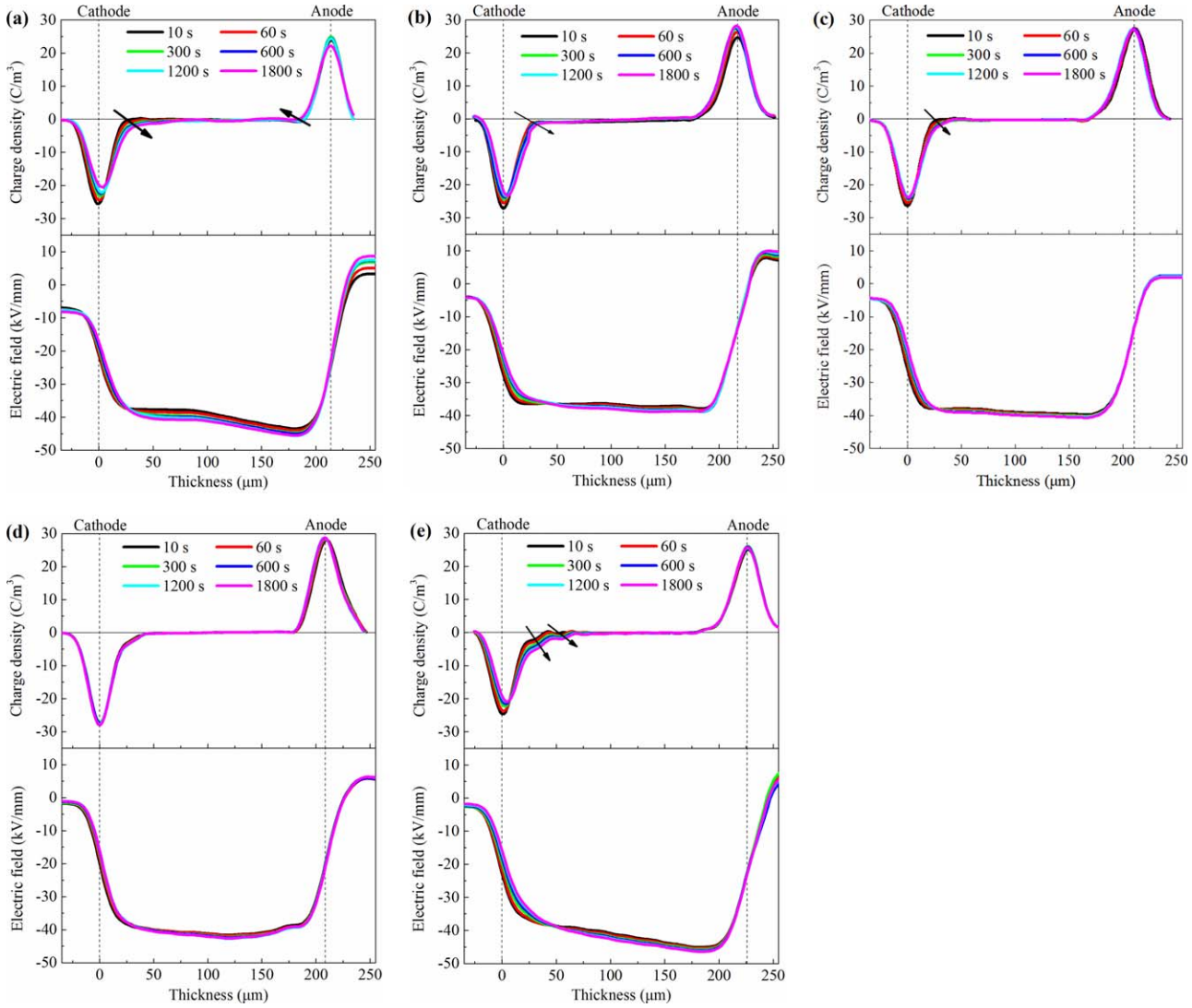

Figure 9. Space charge and corresponding electric field distribution in the MgO/PP/POE nanocomposites filled with surface-modified MgO nanoparticles under a −40 kV/mm dc electric field: (a) 0, (b) 0.5, (c) 1, (d) 3, and (e) 5 phr. [Color figure can be viewed in the online issue, which is available at wileyonlinelibrary.com.]

surface-modified nanoparticles in the polymer matrix can induce space-charge suppression and increase the breakdown strength of nanocomposites.[47,48] Figure 9 illustrates the space-charge distribution and corresponding electrical field profiles within the samples at 30 min after the application of a −40 kV/mm dc electric field. As shown clearly from Figure 9(a), there were large amounts of homogenous charges injected quickly from both electrodes, especially the cathode, in the PP/POE blends. The injected homogenous charges accumulated at the vicinity of the cathode, and the injection depth increased with time. From the electrical field distribution in the PP/POE blends shown in Figure 9(a), the accumulation of space charge caused a serious distortion in the local electric field; this was very unfavorable for insulation applications. The accumulation of space charges in the PP/POE blends were attributed to the large amount of charge-trapping sites introduced at the interface of PP and POE because of the different physical and chemical properties, such as the permittivity, conductivity, charge mobility, and crystal morphology. These trapping sites may have trapped charges injected from the electrodes or originated from impurity ionization, and then, the space-charge accumulation formed.

When the surface-modified MgO nanoparticles were introduced into the PP/POE blends, the space-charge accumulation was effectively suppressed, and the distortion of the electric field was significantly improved. As shown in Figure 8(b,c), there was only a small amount of homogenous charges injected and accumulated in the nanocomposites with 0.5- and 1-phr surface-modified MgO nanoparticles, and the charge injection depth increased slowly with time; this indicated a lower charge injection rate and charge mobility. This was consistent with the results of leakage current and dc volume resistivity of the nanocomposites. When the MgO nanofiller content was 3 phr, the nanocomposites possessed the best space-charge suppression performance, as there was almost no space-charge accumulation, and very little distortion of the electric field inside the samples was observed, as shown in Figure 9(d). The space-charge behavior of the polymer nanocomposites depended on the trapping, detrapping, and transporting characteristics of the charge carriers inside the material. Changes in the charge trap depth, trap density, and charge carrier mobility can all lead to changes in the space-charge accumulation performance. As shown in previous studies,[49,50] the inclusion of nanoparticles in polymers could introduce a large amount of charge trapping sites at the interfacial zones between the nanoparticles and polymer matrix; this has a large influence on the charge-transport behaviors and space-charge accumulation of the nanocomposites.

As shown in Figure 9(e), when the MgO nanofiller content was 5 phr, the effect of space-charge suppression became worse, and a large amount of space charge was injected and accumulated at the cathode; this was even worse than the behavior of the PP/POE blends. This was caused by the large amount of nanoparticle aggregation [shown in Figure 3(e)], which reduced the interfaces between the nanoparticles and polymer matrix, and as a result, the number of trapping sites decreased. Also, the aggregated nanoparticles acted as impurities, and this led to serious space-charge accumulation. So, the space-charge suppression performance became worse at higher loadings of MgO nanoparticles.[26]

CONCLUSIONS

MgO/PP/POE nanocomposites were prepared by melt blending with MgO nanoparticles that were surface-modified with the silane coupling agent KH550 as nanofillers. The effects of the surface-modified MgO nanoparticles on the morphology, crystal structure, mechanical properties, dc breakdown strength, leakage current, dc volume resistivity, and space-charge accumulation characteristics of the nanocomposites were investigated. The scanning electron microscopy images showed that the surface-modified MgO nanoparticles were well dispersed with few aggregates at low loading contents of less than 3 phr; this changed the crystalline phases of PP in the nanocomposites, and the β-phase PP increased significantly. This was beneficial for improving the mechanical properties. A synergistic toughening effect on PP through the introduction of POE and MgO nanoparticles was observed through tensile tests, and the tensile strength and elongation at break of the nanocomposites were evidently improved with less than 1-phr MgO nanoparticles. The optimal content of MgO nanoparticles for improving the dc electrical properties was 3 phr, which exhibited a much higher dc breakdown strength and dc volume resistivity. The enhanced dc electrical characteristics were attributed to the space-charge suppression effect of the surface-modified MgO nanoparticles. The PP/POE blends and MgO/PP/POE nanocomposites all had a stable dielectric permittivity and low dielectric loss tangent; this indicated a broad applicable frequency range. All of these enhancement in the mechanical and electrical properties were closely related to the large interfacial zones and good adhesion properties between the nanoparticles and polymer matrix. Last but not least, the MgO/PP/POE nanocomposite was essentially different from XLPE, as the former is a thermoplastic material that is very easy to be recycled at the end of its lifetime. An ecofriendly recyclable material is undoubtedly a better choice with the increasing pressure for sustainable development and environmental protection. As a result, the MgO/PP/POE nanocomposites are promising and could be applied in many cases, especially for recyclable HVDC cable insulation materials.

ACKNOWLEDGMENTS

This work was supported in part by the National Basic Research Program of China (973 Project) through grant 2014CB239504.

REFERENCES

1. Kango, S.; Kalia, S.; Celli, A.; Njuguna, J.; Habibi, Y.; Kumar, R. *Prog. Polym. Sci.* **2013**, *38*, 1232.
2. Balazs, A. C.; Emrick, T.; Russell, T. P. *Science* **2006**, *314*, 1107.
3. Lewis, T. J. *IEEE Trans. Dielectr. Electr. Insul.* **1994**, *1*, 812.
4. Tanaka, T.; Montanari, G. C.; Mulhaupt, R. *IEEE Trans. Dielectr. Electr. Insul.* **2004**, *11*, 763.
5. Hampton, R. N. *IEEE Electr. Insul. Mag.* **2008**, *24*, 5.

6. Nelson, J. K. Presented at the 2007 IEEE Electrical Insulation Conference and Electrical Manufacturing Expo, Nashville, TN, October 22–24, **2007**.
7. Roy, M.; Nelson, J. K.; MacCrone, R. K.; Schadler, L. S. *J. Mater. Sci.* **2007**, *42*, 3789.
8. Tanaka, T. *IEEE Trans. Dielectr. Electr. Insul.* **2005**, *12*, 914.
9. Guevara-Morales, A.; Taylor, A. C. *J. Mater. Sci.* **2014**, *49*, 1574.
10. Nelson, J. K.; Hu, Y. *J. Phys. D: Appl. Phys.* **2005**, *38*, 213.
11. Zhang, P.; He, J.; Cui, Z. K.; Li, X.; Liu, X.; Zhang, S.; Zhuang, Q.; Han, Z. *Polymer* **2015**, *65*, 262.
12. Wei, J.; Zhang, S.; Liu, X.; Qian, J.; Hua, J.; Li, X.; Zhuang, Q. *J. Mater. Chem. A* **2015**, *3*, 8205.
13. Chen, Y.; Zhang, S.; Liu, X.; Pei, Q.; Qian, J.; Zhuang, Q.; Han, Z. *Macromolecules* **2015**, *48*, 365.
14. Hanley, T. L.; Burford, R. P.; Fleming, R. J.; Barber, K. W. *IEEE Electr. Insul. Mag.* **2003**, *19*, 13.
15. Nitta, K. H.; Shin, Y. W.; Hashiguchi, H.; Tanimoto, S.; Terano, M. *Polymer* **2005**, *46*, 965.
16. Da Silva, A. L. N.; Tavares, M. I. B.; Politano, D. P.; Coutinho, F.; Rocha, M. C. *J. Appl. Polym. Sci.* **1997**, *66*, 2005.
17. Wu, C. L.; Zhang, M. Q.; Rong, M. Z.; Friedrich, K. *Compos. Sci. Technol.* **2002**, *62*, 1327.
18. Zhou, Y.; He, J. L.; Hu, J.; Huang, X. Y.; Jiang, P. K. *IEEE Trans. Dielectr. Electr. Insul.* **2015**, *22*, 673.
19. Montanari, G. C. *IEEE Trans. Dielectr. Electr. Insul.* **2011**, *18*, 339.
20. Huang, X. Y.; Jiang, P. K.; Yin, Y. *Appl. Phys. Lett.* **2009**, *95*, 242905.
21. Tuncer, E.; Sauers, I.; James, D. R.; Ellis, A. R.; Paranthaman, M. P.; Aytuğ, T.; Sathyamurthy, S.; More, K. L.; Li, J.; Goyal, A. *Nanotechnology* **2007**, *18*, 025703.
22. Bittmann, B.; Haupert, F.; Schlarb, A. K. *Ultrason. Sonochem.* **2009**, *16*, 622.
23. Yasmin, A.; Abot, J. L.; Daniel, I. M. *Scr. Mater.* **2003**, *49* 81.
24. Zha, J. W.; Sun, F.; Wang, S. J.; Wang, D.; Lin, X.; Chen, G.; Dang, Z. M. *J. Appl. Phys.* **2014**, *116*, 134104.
25. Ma, D.; Hugener, T. A.; Siegel, R. W.; Christerson, A.; Mårtensson, E.; Önneby, C.; Schadler, L. S. *Nanotechnology* **2005**, *16*, 724.
26. Peng, S. M.; He, J. L.; Hu, J.; Huang, X. Y.; Jiang, P. K. *IEEE Trans. Dielectr. Electr. Insul.* **2015**, *22*, 1512.
27. Lomax, J. F.; Fontanella, J. J.; Edmondson, C. A.; Wintersgill, M. C.; Wolak, M. A.; Westgate, M. A.; Lomax, E. A.; Lomax, P. Q.; Bogle, X.; Rúa, A.; Greenbaum, S. G. *J. Appl. Phys.* **2014**, *115*, 104103.
28. Singh, B. P.; Singh, D.; Mathur, R. B.; Dhami, T. L. *Nanoscale Res. Lett.* **2008**, *3*, 444.
29. Huang, X. Y.; Liu, F.; Jiang, P. K. *IEEE Trans. Dielectr. Electr. Insul.* **2010**, *17*, 1697.
30. Meille, S. V.; Ferro, D. R.; Brückner, S.; Lovinger, A. J.; Padden, F. J. *Macromolecules* **1994**, *27*, 2615.
31. Fillon, B.; Thierry, A.; Wittmann, J. C.; Lotz, B. J. Polym. Sci. Part B: Polym. Phys. **1993**, *31*, 1407.
32. Garbarczyk, J.; Paukszta, D. *Colloid Polym. Sci.* **1985**, *263*, 985.
33. Grein, C.; Plummer, C. J. G.; Kausch, H. H.; Germain, Y.; Béguelin, P. *Polymer* **2002**, *43*, 3279.
34. Zhang, P.; Liu, X.; Li, Y. *Mater. Sci. Eng. A* **2006**, *434*, 310.
35. Machado, G.; Denardin, E. L. G.; Kinast, E. J.; Gonçalves, M. C.; De Luca, M. A.; Teixeira, S. R.; Samios, D. *Eur. Polym. J.* **2005**, *41*, 129.
36. Kordas, G. *J. Mater. Chem.* **2000**, *10*, 1157.
37. Galeski, A. *Prog. Polym. Sci.* **2003**, *28*, 1643.
38. Wu, C. L.; Zhang, M. Q.; Rong, M. Z.; Friedrich, K. *Compos. Sci. Technol.* **2005**, *65*, 635.
39. Hong, R. Y.; Fu, H. P.; Zhang, Y. J.; Liu, L.; Wang, J.; Li, H. Z.; Zheng, Y. *J. Appl. Polym. Sci.* **2007**, *105*, 2176.
40. Lee, S. H.; Kontopoulou, M.; Park, C. B. *Polymer* **2010**, *51*, 1147.
41. Zhang, L.; Zhou, Y. X.; Cui, X.; Sha, Y. C.; Le, T. H.; Ye, Q.; Tian, J. H. *IEEE Trans. Dielectr. Electr. Insul.* **2014**, *21*, 1554.
42. Zhang, Y.; Lewiner, J.; Alquie, C.; Hampton, N. *IEEE Trans. Dielectr. Electr. Insul.* **1996**, *3*, 778.
43. Montanari, G. C.; Fabiani, D.; Palmieri, F.; Kaempfer, D.; Thomann, R.; Mulhaupt, R. *IEEE Trans. Dielectr. Electr. Insul.* **2004**, *11*, 754.
44. Ishimoto, K.; Kanegae, E.; Ohki, Y.; Tanaka, T.; Sekiguchi, Y.; Murata, Y.; Reddy, C. C. *IEEE Trans. Dielectr. Electr. Insul.* **2009**, *16*, 1735.
45. Takada, T.; Hayase, Y.; Tanaka, Y. *IEEE Trans. Dielectr. Electr. Insul.* **2008**, *15*, 152.
46. Hong, J. I.; Schadler, L. S.; Siegel, R. W.; Mårtensson, E. *Appl. Phys. Lett.* **2003**, *82*, 1956.
47. Ju, S. T.; Zhang, H.; Chen, M. J.; Zhang, C.; Chen, X.; Zhang, Z. *Compos. A* **2014**, *66*, 183.
48. Dou, X.; Liu, X.; Zhang, Y.; Feng, H.; Chen, J. F.; Du, S. *Appl. Phys. Lett.* **2009**, *95*, 132904.
49. Tian, F.; Lei, Q. Q.; Wang, X.; Wang, Y. *Appl. Phys. Lett.* **2011**, *99*, 142903.
50. Han, B.; Wang, X.; Sun, Z.; Yang, J. M.; Lei, Q. Q. *Appl. Phys. Lett.* **2013**, *102*, 012902.